Actin Dynamics in Papilla Cells of *Brassica rapa* during Self- and Cross-Pollination[1][W]

Megumi Iwano*, Hiroshi Shiba, Kyoko Matoba, Teruhiko Miwa, Miyuki Funato, Tetsuyuki Entani, Pulla Nakayama, Hiroko Shimosato, Akio Takaoka, Akira Isogai, and Seiji Takayama

Graduate School of Biological Sciences, Nara Institute of Science and Technology, Ikoma, Nara 630–0101, Japan (M.I., H.S., T.M., M.F., T.E., P.N., H.S., A.I., S.T.); and Research Center for Ultra-High Voltage Electron Microscopy, Osaka University, Suita, Osaka 565–0781, Japan (K.M., A.T.)

The self-incompatibility system of the plant species *Brassica* is controlled by the *S*-locus, which contains *S-RECEPTOR KINASE* (*SRK*) and *S-LOCUS PROTEIN11* (*SP11*). *SP11* binding to *SRK* induces *SRK* autophosphorylation and initiates a signaling cascade leading to the rejection of self pollen. However, the mechanism controlling hydration and germination arrest during self-pollination is unclear. In this study, we examined the role of actin, a key cytoskeletal component regulating the transport system for hydration and germination in the papilla cell during pollination. Using rhodamine-phalloidin staining, we showed that cross-pollination induced actin polymerization, whereas self-pollination induced actin reorganization and likely depolymerization. By monitoring transiently expressed green fluorescent protein fused to the actin-binding domain of mouse talin, we observed the concentration of actin bundles at the cross-pollen attachment site and actin reorganization and likely depolymerization at the self-pollen attachment site; the results correspond to those obtained by rhodamine-phalloidin staining. We further showed that the coat of self pollen is sufficient to mediate this response. The actin-depolymerizing drug cytochalasin D significantly inhibited pollen hydration and germination during cross-pollination, further emphasizing a role for actin in these processes. Additionally, three-dimensional electron microscopic tomography revealed the close association of the actin cytoskeleton with an apical vacuole network. Self-pollination disrupted the vacuole network, whereas cross-pollination led to vacuolar rearrangements toward the site of pollen attachment. Taken together, our data suggest that self- and cross-pollination differentially affect the dynamics of the actin cytoskeleton, leading to changes in vacuolar structure associated with hydration and germination.

Many families of flowering plants have evolved genetically controlled self-incompatibility (SI) systems to inhibit self-fertilization. SI in *Brassica* is controlled by a single, highly polymorphic locus, the *S*-locus (Bateman, 1955). In this SI system, when a stigma and an interacting pollen grain have an identical *S*-haplotype, the pollen is identified as incompatible (self) and pollen germination or pollen tube growth is inhibited. Conversely, when a compatible (cross) pollen grain adheres to a papilla cell of the stigma, the pollen grain is hydrated and germinates a pollen tube. The pollen tube penetrates the surface of the papilla cell and enters the style. Finally, sperm cells in the pollen tube are released into the embryo sac and fertilization occurs.

During self-pollination, binding of a pollen component, *S-LOCUS PROTEIN11* (*SP11*)/*S-LOCUS CYSRICH PROTEIN* (*SCR*) determinant (Schopfer et al., 1999; Takayama et al., 2000; Shiba et al., 2001), to a stigmatic recognition component, *S-RECEPTOR KINASE* (*SRK*; Takasaki et al., 2000; Silva et al., 2001), induces *SRK* autophosphorylation and generation of a signaling cascade leading to germination arrest (Takayama et al., 2001; Takayama and Isogai, 2005). Additional components involved in the signaling cascade leading to inhibition of self-fertilization include ARC1, an arm repeat-containing protein with E3 ubiquitin ligase activity (Stone et al., 1999, 2003), and the membrane-anchored *M*-locus protein kinase (Murase et al., 2004). However, the mechanism used by the papilla cell to block self-pollen germination and to facilitate cross-pollen germination remains unclear.

During compatible pollination, the papilla cell is thought to actively transport water, calcium, and boron, factors essential for normal pollen germination, into a pollen grain. Furthermore, pollen tube penetration and elongation into the papilla cell wall likely leads to cell wall loosening or reorganization. However, the mechanisms controlling the provision of water, calcium, and boron to a pollen tube and papilla cell wall reorganization are unclear. A previous electron microscopic study showed that many secretory vesicles were seen at the site of pollen attachment in papilla cells during cross-pollination (Elleman and

[1] This work was supported by Grants-in-Aid for Special Research on Priority Areas (grant nos. 16GS0316 and 18075008), Grants-in-Aid for Special Research (C; grant no. 17570037) from the Ministry of Education, Culture, Sports, Science and Technology of Japan, and by "Nanotechnology Support Project of the Ministry of Education, Culture, Sports, Science and Technology (MEXT), Japan" at the Research Center for Ultrahigh Voltage Electron Microscopy, Osaka University.

* Corresponding author; e-mail m-iwano@bs.naist.jp; fax 81–743–72–5459.

The author responsible for distribution of materials integral to the findings presented in this article in accordance with journal policy described in the Instructions for Authors (http://www.plantphysiol.org) is: Megumi Iwano (m-iwano@bs.naist.jp).

[W] The online version of this article contains Web-only data.
www.plantphysiol.org/cgi/doi/10.1104/pp.106.095273

Dickinson, 1996). A similar phenomenon was seen at the site of infection during plant cell-pathogen interactions and this appears to be regulated by the actin cytoskeleton (Kobayashi et al., 1992, 1994; Skalamera and Heath, 1998; Takemoto et al., 2003; Takemoto and Hardham, 2004). Furthermore, polymerization and depolymerization of actin filaments are involved in tip growth of pollen tubes and root hairs, cytoplasmic streaming, cellular morphogenesis, and cell division (Miller et al., 1999; Staiger, 2000; Hepler et al. 2001; Wasteneys and Galway, 2003; Shimmen and Yokota, 2004). Additionally, the actin cytoskeleton undergoes reorganization in response to external stimuli, such as gravity and hormones (Kandasamy et al., 2001; Sun et al., 2004). Therefore, the physiological changes seen in the papilla cell may be directly or indirectly related to changes in actin cytoskeleton dynamics during pollen germination.

To test this hypothesis, we examined whether the actin cytoskeleton in the papilla cell plays an important role in pollen germination during self- and cross-pollination. We visualized and compared the configurations of actin filaments in stigmatic papilla cells before and after self- and cross-pollination by staining actin filaments with rhodamine-phalloidin and by the transiently expressing GFP fused to the actin-binding domain of mouse talin (mTalin) in a papilla cell. Furthermore, we examined the effects of the cross- and self-pollen coat on actin cytoskeletal structure, as well as the effects of cytochalasin D (CD), an actin-depolymerizing drug, on actin cytoskeletal structure in cross- and self-pollinated papilla cells. Finally, we compared the three-dimensional (3D) configurations of vacuolar structures associated with actin filaments in papilla cells before and after self- and cross-pollination by tomography using ultra-high-voltage electron microscopy (ultra-HVEM).

RESULTS

Actin Cytoskeleton in Stigmatic Papilla Cells of *Brassica rapa*

We examined actin cytoskeleton organization in these cells by fixing stigmas before and after pollination and staining actin filaments with rhodamine-phalloidin. Images were captured by confocal microscopy and images obtained along the optical *z* axis through a complete cell were reconstructed (Fig. 1, A–F). Prior to pollination, actin bundles were arranged along the longitudinal axis of the papilla cell (Fig. 1A). These actin bundles were distinct from those surrounding the nucleus and the actin filaments at the apical region of papilla cells were finer than those found at the central region.

To examine whether the organization of actin filaments changed during cross- and self-pollination, papillar actin microfilaments were observed 30 min, 1 h, and 1.5 h after cross- or self-pollination. Thirty minutes after cross-pollination, a time when most pollen grains begin to hydrate, we observed distinct actin bundles at the apical region (Fig. 1B, arrows); 1 h after cross-pollination, the period when many pollen grains germinate and begin to penetrate the papilla cell wall, many actin bundles were seen both along the longitudinal axis and concentrated at the pollen germination site (Fig. 1C, arrows). In contrast, during self-pollination, actin filaments at the apical region decreased over time and rearrangement of the actin filaments around the nuclei was not apparent 30 min (Fig. 1D) or 1 h (Fig. 1E) after pollination; 1.5 h after pollination, the total amount of actin filaments further decreased (Fig. 1F). These experiments were performed five times with reproducible results. Therefore, by rhodamine-phalloidin staining in stigmatic papilla cells, actin filaments increased during cross-pollination and decreased during self-pollination.

Quantitative Analysis of Actin Filament Rearrangement during Cross- and Self-Pollination

To quantitatively examine the extent of actin filament rearrangement at the apical region during cross- and self-pollination, we measured the fluorescence intensity of a cross-section of a papilla cell (Fig. 1, A–F, bars and graphs). Large peaks indicate the presence of actin bundles and small peaks represent fine actin filaments. During cross-pollination, both the magnitude and number of large peaks increased (Fig. 1, B and C). In contrast, during self-pollination, a large peak was not detected and the number of small peaks also decreased (Fig. 1, D and E). These quantitative results are consistent with the data shown in Figure 1. We next randomly selected 50 papilla cells from individual experiments and calculated the mean fluorescence intensities at the apical region of each papilla cell. In the papilla cells exposed to cross pollen, the mean fluorescence intensity of actin filaments increased significantly 1 and 1.5 h after pollination, but decreased significantly in cells undergoing self-pollination 1 and 1.5 h after pollination (Fig. 1G). Taken together, these data suggest that actin polymerization is induced by cross-pollination, whereas self-pollination leads to actin reorganization and likely depolymerization.

In Vivo Monitoring of the Actin Cytoskeleton with GFP-mTalin

To examine actin dynamics over time in a single papilla cell during cross- and self-pollination, GFP-mTalin, which has an F-actin-binding domain, was transiently expressed in papilla cells by the particle bombardment method. Using a micromanipulator, a cross- or a self-pollen grain was placed on a papilla cell expressing GFP-mTalin and rearrangement of actin filament in the papilla cell was monitored over time.

Before pollination, fine actin filaments, which were not visualized by rhodamine-phalloidin staining, were observed at the apical region of the papilla cell. Consistent with the previous rhodamine-phalloidin experiments,

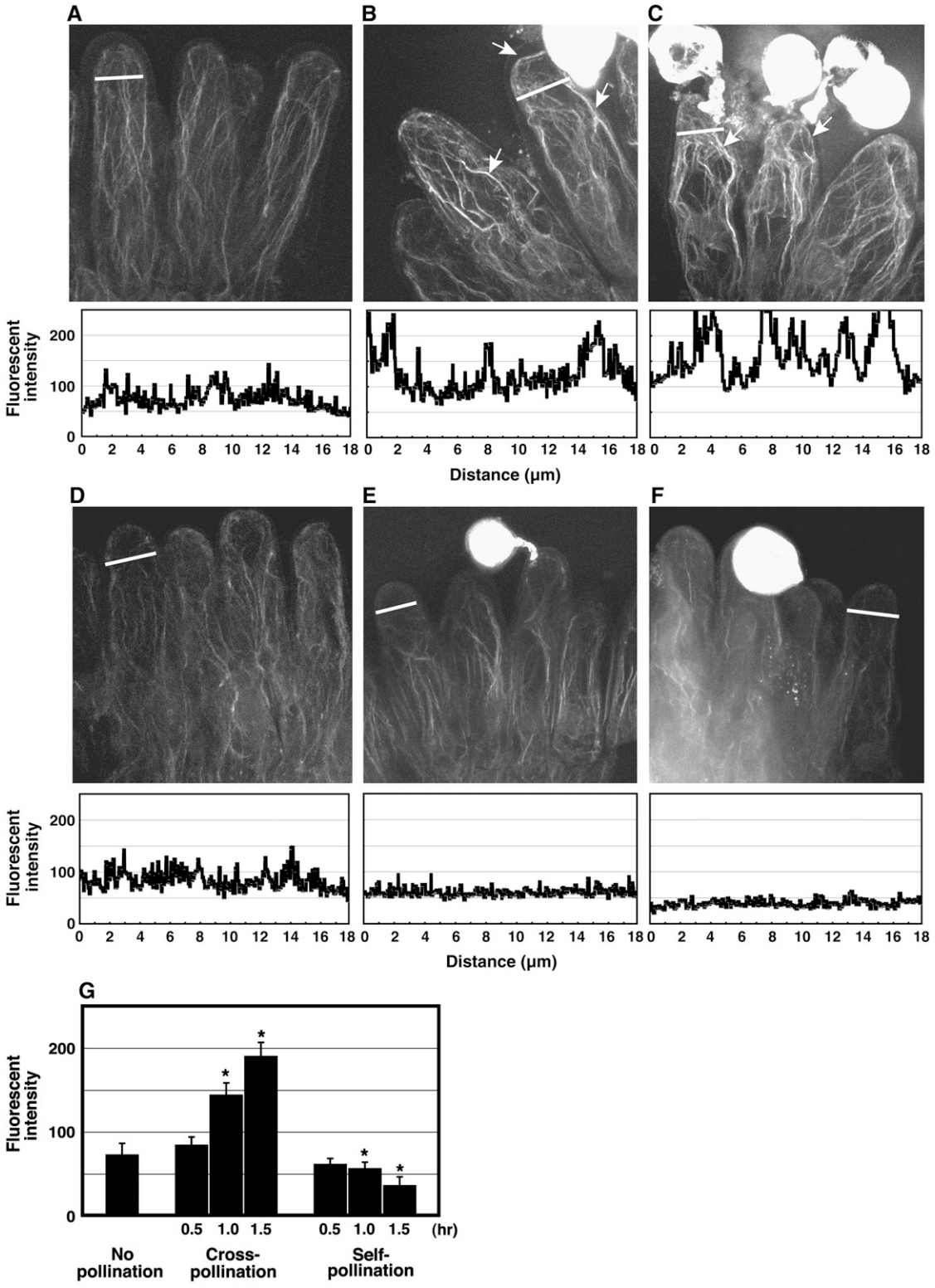

Figure 1. Cross-pollination induces actin cytoskeleton rearrangements, whereas self-pollination disrupts actin structure. Stacked images of rhodamine-phalloidin stained papilla cells before pollination (A), 30 min (B), or 1 h (C) after cross-pollination are shown. Thirty minutes after cross-pollination, few actin bundles became visible in 63% of observed papilla cells (117/185). After 1 h, actin bundles were more pronounced (arrows) in 82% of observed papilla cells (141/171). The number of actin filaments increased at the apical region. No changes were seen 30 min after self-pollination in 93% of the papilla cells (15/213; D), and the number of actin filaments decreased at the apical region in 51% of papilla cells (112/218) 1 h after self-pollination (E).

however, actin bundles were only rarely seen at the apical region with mTalin-GFP (Fig. 2, A and E). Thirty minutes after cross-pollination, the time at which pollen hydration begins, actin bundles, focused at the pollen grain, appeared in the apical region of the papilla cell (Fig. 2, B and F) and these distinct actin bundles remained focused on the point of pollen grain attachment during pollen hydration (Fig. 2, C and G); 1.5 h after pollination, when the pollen has typically germinated and begun to penetrate into a papilla cell, the direction of the actin bundles changed around the pollen tube (Fig. 2, D and H). Furthermore, prominent actin bundles focused at the penetration site were detected (Fig. 2, T and X). On the contrary, hydration of self-pollen grains only rarely occurred by 1.5 h after pollination. Additionally, under conditions of self-pollination, the number of apical actin filaments decreased at 1 h and prominent actin bundles never formed (Fig. 2, I–P). Finally, the number of fine actin filaments gradually decreased. Thus, the real-time visualization of the dynamics of actin rearrangements following cross- and self-pollination was consistent with data obtained using fixed cells and rhodamine-phalloidin staining, although pollen hydration and germination during cross-pollination were slightly delayed in this system for unknown reasons.

Alterations in the Actin Cytoskeleton Induced by the Pollen Coat of Cross- and Self-Pollen Grains

The pollen coat from self-pollen grains induces a self-incompatible response in papilla cells (Stephenson et al., 1997; Takayama et al., 2000). To examine whether the pollen coat alone from cross- and self-pollen grains induces actin reorganization, we monitored the organization of actin filaments in papilla cells over time following application of the pollen coat to the GFP-mTalin-expressing papilla cells.

After cross-pollen coat adhesion, the number of actin filaments gradually increased at the apical region and actin bundles were observed after 20 min (Fig. 2, Q–S). Thus, components of the cross-pollen coat alone were capable of mediating actin polymerization and bundle formation seen in papilla cells during cross-pollination. In contrast, after self-pollen coat adhesion, the number of actin filaments quickly decreased at the apical region and only few filaments were observed after 20 min (Fig. 2, U–W). These data further confirm the importance of the pollen coat in inducing alterations in the actin cytoskeleton in papilla cells during cross- or self-pollination.

Effects of CD on Pollination

Actin polymerization could be directly involved in the hydration and germination of the pollen grain. To test this hypothesis, we examined the effects of CD, an actin-depolymerizing drug, on pollination. For this experiment, pistils were excised and the cutting edge was soaked in a solution containing 100 μM CD for 4 h. Following fixation, pistils were stained with rhodamine-phalloidin. We detected prominent actin bundle fragmentation in the pistils treated with CD compared with those soaked in the control solution containing dimethyl sulfoxide (Fig. 3, A and B). Some pistils soaked in CD (100 μM) for 4 h were pollinated with cross- or self-pollen grains for 2 h and the pollinated pistils were then fixed and stained with rhodamine-phalloidin. Very little germination occurred during either cross- or self-pollination in the presence of CD (data not shown). Therefore, 100 μM CD inhibited pollen grain germination.

We next examined whether germination inhibition by CD was dose dependent. We soaked the cut pistil edge in different concentrations of CD for 4 h and examined hydration and germination following pollen grain addition using a micromanipulator (Fig. 2C). When a cross-pollen grain was attached to a papilla cell exposed to 10 μM CD, pollen hydration and germination were not inhibited. However, both pollen hydration and germination were significantly inhibited by 50 μM CD and germination was completely inhibited by 100 μM CD. The ability of CD to inhibit both pollen hydration and germination suggests that actin polymerization is required for these processes.

Ultra-HVEM Tomography of Vacuolar Structure in Papilla Cells before Pollination

In Figure 2, we described the formation of actin bundles directly adjacent to the site of adhesion of germinated cross pollen in papilla cells transiently expressing GFP-mTalin. When cells were examined with transmission electron microscopy, we found that the apical region of papilla cells was occupied with large, small, and tubular vacuoles (Fig. 4A). To better understand the relationship between the actin cytoskeleton and the vacuolar structure, we performed tomographic analysis using ultra-HVEM observing 2- to 3-μm-thick longitudinal sections of papilla cells. Figure 4B is a projection image of a typical papilla cell before pollination. Large vacuoles occupied a large portion of the papilla cell and these were surrounded by complex tubular or round vacuoles. Despite the detail provided by these

Figure 1. (*Continued.*)
Furthermore, the number of actin filaments decreased throughout the entire cell in 54% (67/124) of examined papilla cells 1.5 h after self-pollination (E and F). Graphs under each photograph indicate the fluorescence intensity of the actin cytoskeleton at the position indicated by the bar. The horizontal axis indicates the distance from the left to the right side of each bar. The vertical axis indicates the rhodamine-phalloidin fluorescence intensity at that location. G, Fluorescence intensity of the actin cytoskeleton at the tip of papilla cells stained with rhodamine-phalloidin. Fluorescence intensity of the apical regions of 50 individual cells was measured and the mean ± SD is shown for each pollination condition; asterisks indicate values significantly different ($P < 0.05$) from the control determined by Student's *t* test.

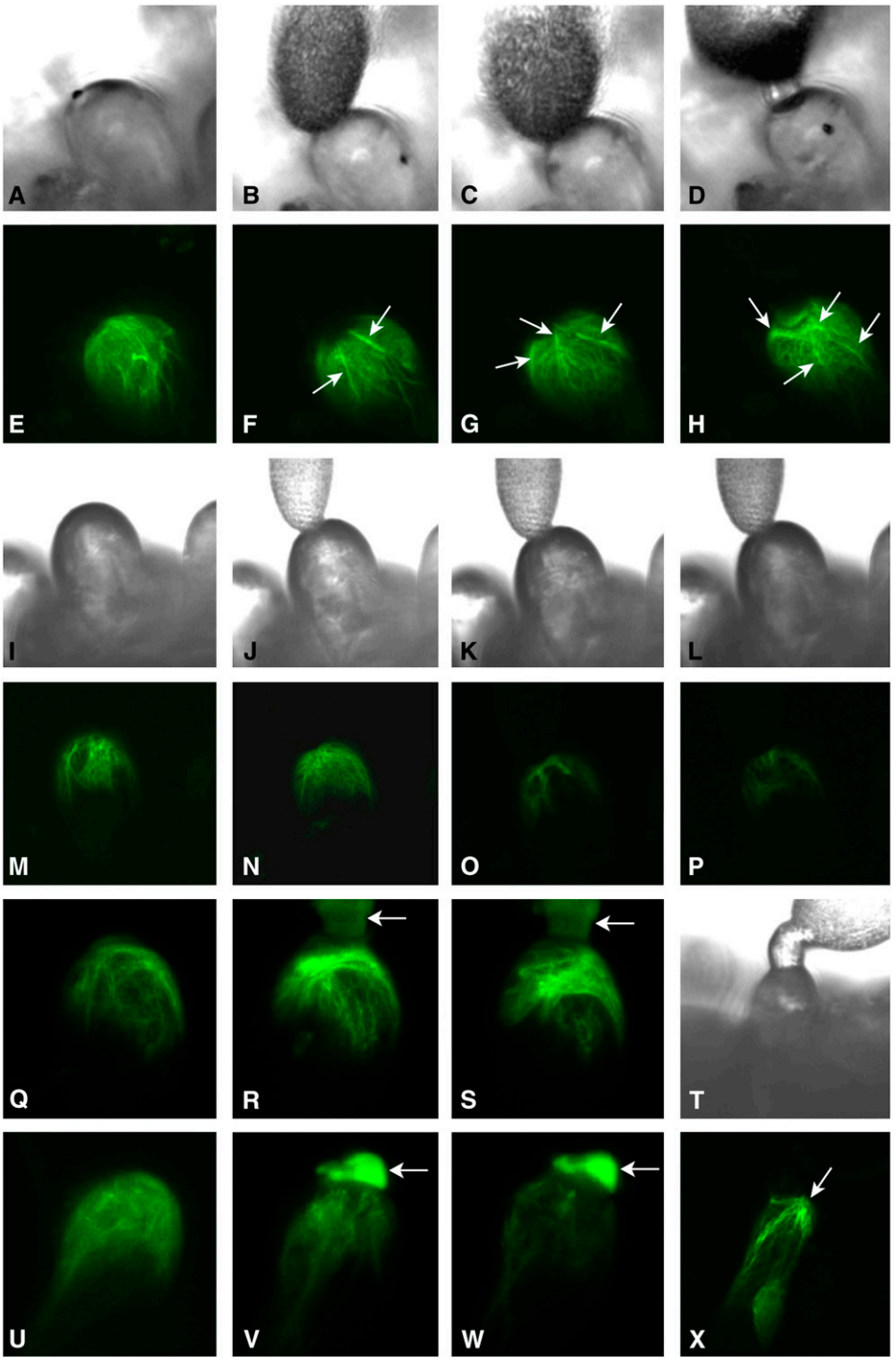

Figure 2. Alterations in the actin cytoskeleton during cross- and self-pollination and after adhesion of cross- or self-pollen coats visualized in cells expressing GFP-mTalin. Bright-field (A–D and T) and fluorescent images (E–H and X) of papilla cells expressing GFP-mTalin before (A and E) and after cross-pollination are shown. Thirty minutes after pollination (B and F), hydration has begun and actin bundles (arrows) are visible at the site of pollen contact. These actin bundles became more pronounced after 1 h (C and G). Actin bundles are visible around the penetrating pollen tube 1.5 h after pollen addition (D and H); 1.5 h after cross-pollination, actin bundles are concentrated at the site of pollen tube penetration (T and X). For this experiment, 12 papilla cells were examined. Pollen germination and penetration were successful on one-half (6/12) of the papilla cells and actin bundles were observed in all papilla cells with germinated pollen (6/6). Bright-field (I–L) and fluorescent images (M–P) of papilla cells expressing GFP-mTalin before (I and M) and after self-pollination are shown. No changes are seen 30 min after pollination (J and N) and decreased fluorescence is seen 1 h (K and O) and 1.5 h (L and P) after self-pollination. Fifteen cells were examined and in 78% of cells (12/15) a decrease in the number of actin filaments was observed. Cells expressing GFP-mTalin were treated with cross- or self-pollen coats and the actin cytoskeleton was monitored by GFP-mTalin fluorescence. Actin filaments are seen before pollen coat adhesion (Q and U). The increase in the number of filaments can be detected at 10 min (R) and 20 min (S) after cross-pollen coat addition and the decrease in the number of actin filaments can be seen at 10 (V) and 20 min (W) after self-pollen coat addition. Arrows indicate the pollen coats. These changes in the actin cytoskeleton were seen in 70% (7/10) and 75% (9/12) of the papilla cells examined after adhesion of cross- and self-pollen coat, respectively.

images, they did not reveal the 3D structure of vacuoles. To accomplish this, we performed tomographic analysis of ultra-HVEM images. In this approach, images of 2-μm-thick sections were taken at 3,000× magnification from +60° to −60° at 2° intervals around two orthogonal axes. The images were then aligned and the tomographic volumes were reconstructed using IMOD software. In the reconstructed image of a papilla cell before pollination, prominent tubular vacuoles were seen near the large vacuoles (Fig. 4C, small arrows). Additionally, tubular vacuoles were directly connected to large vacuoles (Fig. 4C, large arrows) or in a branching structure (Fig. 4C, asterisk). Reconstruction of the 3D tubular vacuoles using IMOD software revealed a branching vacuolar network connected with the large vacuole at several locations (Fig. 4D; Supplemental Video S1).

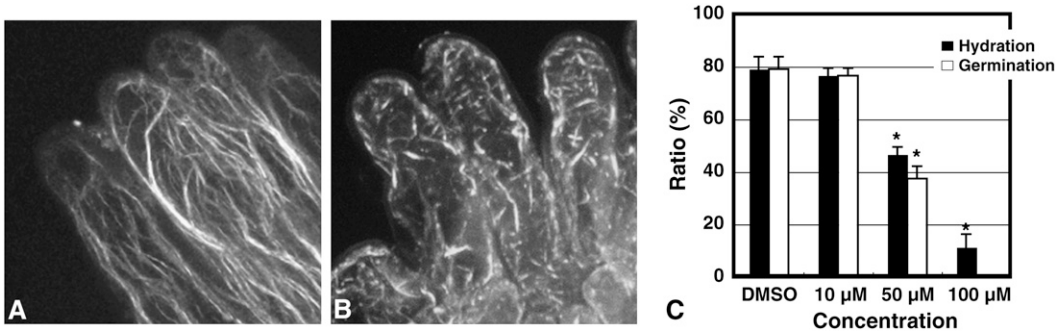

Figure 3. CD disrupts the papilla cell actin cytoskeleton, pollen grain hydration, and germination following cross-pollination. A, Control cells untreated with 100 μM CD and stained with rhodamine-phalloidin as in Figure 1. B, Cells treated with 100 μM CD and stained with rhodamine-phalloidin as in Figure 1. C, Papilla cells were treated with the indicated concentrations of CD for 4 h prior to pollination. At 1.5 h after cross-pollen application, the extent of pollen grain hydration and germination was observed by light microscopy. Data shown represent the means ± SD of 50 cells from five independent experiments; asterisks indicate values significantly different ($P < 0.05$) from the control determined by Student's *t* test.

3D Vacuolar Structure in Papilla Cells after Cross- and Self-Pollination by Ultra-HVEM

At 1 h after cross-pollination, some pollen grains in the stigma had begun to germinate and the remaining pollen grains were hydrated when examined by light microscopy. To examine this process in more detail, we performed tomography on papilla cells with attached germinated pollen grains. In a typical papilla cell after cross-pollination (Fig. 4E), tubular vacuoles coexisted with large vacuoles and they were morphologically similar to cells prior to pollination (Fig. 4D). However, after cross-pollination, a network of elongated and large vacuoles appeared to be directed to the pollen grain attachment site formed below the plasma membrane adjacent to the germinated pollen grain.

In contrast to the findings with cross-pollination, we detected no hydrated or germinated pollen grains on the papilla cells at 1 h after self-pollination by light microscopy. When papilla cells were examined by ultra-HVEM tomography following self-pollination, few elongated vacuoles were seen near the plasma membrane and apical vacuoles appeared fragmented (Fig. 4F). Thus, the 3D structure of the vacuolar network following self-pollination substantially differed from that seen either before pollination or after cross-pollination. Self-pollination induces changes in the vacuolar structure rather than maintaining a preexisting structure in papilla cells.

Effect of CD on the 3D Vacuolar Structure of Papilla Cells

The actin-depolymerizing drug CD disrupted actin bundles and inhibited hydration and germination of pollen grains during cross-pollination (Fig. 3). To examine changes in the vacuolar structure of papilla cells following CD treatment, pistil edges were incubated in 50 μM CD for 3 h and stigma were then prepared for thick-section ultra-HVEM tomography. In CD-treated cells, globular vacuoles surrounded large vacuoles and some connections between these vacuoles were seen (Fig. 4G). However, no tubular vacuoles were seen near the large vacuoles in CD-treated cells and this resembled the appearance of self-pollinated papilla cells. In addition, no large vacuoles localized near the cell membrane. These features were common in CD-treated cells, but were not observed in control, dimethyl sulfoxide-treated cells. Thus, it seems that the appearance of CD-treated cells is close to that of self-pollinated cells.

DISCUSSION

Using both rhodamine-phalloidin staining and real-time monitoring of actin behavior by GFP-mTalin, we precisely visualized the configuration of actin filaments in papilla cells after cross- and self-pollination. In this study, we showed that actin polymerization and bundle formation were promoted by cross-pollination and actin reorganization, most likely depolymerization, occurred after self-pollination. These results are not consistent with a previous report (Dearnaley et al., 1999), but this is likely due to the differences in techniques used to stain actin filaments. In this study, all stigma were treated, frozen, and crushed in liquid nitrogen and permeabilized with 0.05% Tween 20 in Tris-buffered saline containing dithiothreitol for 24 h prior to actin staining. This comprehensive protocol enhances visualization of actin filaments. Differences in sensitivity and/or structure preservation could explain the discrepancies between studies.

Cross-pollination proceeds in an ordered fashion, beginning with pollen adhesion and eventual hydration, germination, and pollen tube penetration into a papilla cell. Actin bundles formed at the apical region of papilla cells during hydration and these bundles, focused at the site of pollen grain attachment, were present during pollen germination and penetration. Treatment of cells with CD, an inhibitor of actin polymerization, induced actin filament fragmentation and

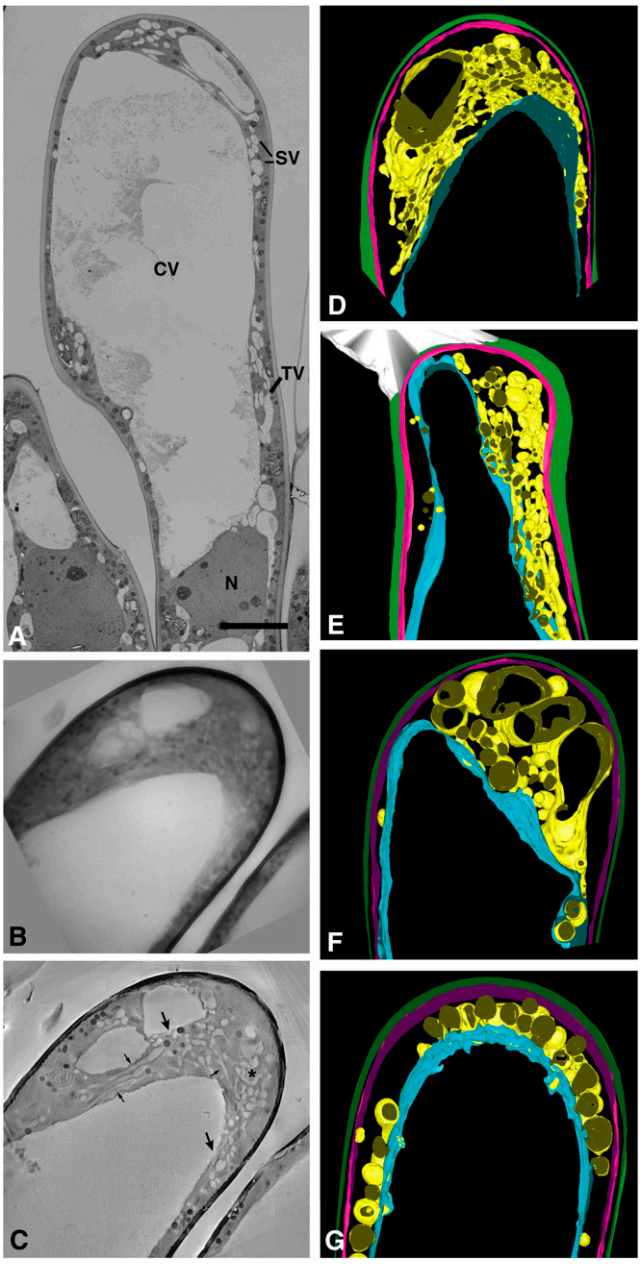

Figure 4. Vacuolar structure in a papilla cell prior to pollination and after cross- and self-pollination. A, Unpollinated papilla cells were observed using transmission electron microscopy accelerated at 75 kV. Small, tubular vacuoles surround the central vacuole. The bar represents 10 μm. CV, Central vacuole; TV, tubular vacuole; SV, small vacuole; N, nucleus. B to D, 3D reconstruction of vacuoles in a typical papilla cell before pollination. Two-micrometer-thick longitudinal sections of papilla cells were observed using ultra-HVEM. B, Projection image at 0° where large vacuoles occupy a large portion of the papilla cell and these were surrounded by complex tubular or round vacuoles. C, Reconstructed image of B. Prominent tubular vacuoles were seen near the large vacuoles (black arrows). Additionally, tubular vacuoles were directly connected to large vacuoles (large arrow) or in a branching structure (asterisk). D, Reconstruction of the 3D tubular vacuoles using IMOD software. A branching vacuolar network (yellow) was connected to the large vacuole (blue) at several locations. Cell surface and cell membrane are shown in green and pink, respectively. The complex network consisting of large and tubular vacuoles was seen in 84% (210/251) of the papilla cells examined. E, 3D reconstruction representative of the altered vacuolar 3D structure following cross-pollination and pollen germination. At the apical region of the papilla cell, an elongated central vacuole (blue) accumulated adjacent to the site of germinated pollen grain attachment. A network of tubular vacuoles surrounds this site and forms a network continuous with a large central vacuole. Pollen tube is shown in white. Pollen germination occurred in 15% (32/205) of papilla cells examined and changes in the vacuole network were seen in 91% cells (29/32) of the cells. F, 3D reconstruction of a papilla cell after self-pollination. At the apical region of the papilla cell, many globular vacuoles (yellow) and few tubular vacuoles are seen. An elongated central vacuole, as in A, is not observed. Of 239 observed cells, 67% cells (161/239) exhibited changes consistent with those shown here. G, CD disrupts the vacuolar 3D structure. Large vacuoles (blue) are surrounded by globular vacuoles (yellow). Tubular vacuoles and elongated vacuoles are not observed. This configuration was observed in 100% (178/178) of papilla cells examined.

inhibited pollen hydration and germination. Actin bundle formation during cross-pollination and inhibition of cross-pollination by CD suggests that the formation of actin bundles in the papilla cell is indispensable for pollen hydration and germination.

In *Brassica*, *SP11/SCR* in the pollen coat of self-pollen grains induces the SI to arrest pollen hydration and germination (Takayama et al., 2000). It is thought that *SP11/SCR* binds to *SRK* and induces *SRK* autophosphorylation to initiate the SI signaling cascade (Kachroo et al., 2001; Takayama et al., 2001). *SP11/SCR* is secreted by the tapetum cells in the anther and associates with the pollen surface. During pollination, *SP11/SCR* is transported from the pollen surface to the papilla cell via the pollen coat, leading to penetration of the papilla cell wall (Iwano et al., 2003). In this study, actin reorganization and likely depolymerization was observed 1 h after self-pollination and the pollen coat alone from self-pollen grains induced these configuration changes. When considered with our previous results, these data suggest that actin reorganization and likely depolymerization are involved in the SI response of papilla cells and occur downstream of *SRK* autophosphorylation.

The situation is reversed during cross-pollination. Actin polymerization was observed 1 h after cross-pollination and the pollen coat alone was responsible for this effect. Furthermore, inhibition of actin polymerization prevented pollen germination. Taken together, these data suggest that the pollen coat initiates a signaling cascade leading to changes in the actin cytoskeleton. Altered actin polymerization may be directly responsible for or coincident with initiation of cross-pollination.

In this study, we visualized the 3D structure of vacuoles in the papilla cell by ultra-HVEM tomography. Vacuolar structures are traditionally visualized by GFP imaging (Mitsuhashi et al., 2000; Saito et al., 2002; Kutsuna et al., 2003; Reisen et al., 2005) and HVEM tomography is typically performed on thin, 0.5-μm sections (Segui-Simarro et al., 2004). However, in this

study, we examined 2- to 3-μm-thick sections using ultra-HVEM with acceleration energies approaching 2,000 kV to reconstruct the 3D network of the large vacuole and tubular vacuoles. Using this technique, we determined that the vacuolar network consists of large, globular, and tubular vacuoles located at the apical region of the papilla cells. The conformation of the vacuolar network changed after cross-pollination, extending toward the pollen attachment site. In contrast, the vacuolar structure after self-pollination was substantially different and resembled the vacuolar network in cells treated with CD; an elongated central vacuole and tubular network at the apical region of the papilla cell were rarely observed. Therefore, this correlation between actin bundle organization and vacuolar structure suggests that actin bundles regulate the structure and the positioning of vacuoles in papilla cells after cross- and self-pollination. The vacuole stores many different compounds and inorganic ions and the tonoplast (vacuolar membrane) contains several different transport systems, including proton pumps such as H^+-ATPase and H^+-pyrophosphatase, transporters such as Ca^{2+}-ATPase, Ca^{2+}/H^+ antiporter, and Na^+/H^+ antiporter, and water channels (aquaporins). These transport proteins regulate ion concentration and turgor pressure in plant cells (Maeshima, 2001). Therefore, the actin cytoskeleton may regulate vacuolar structure to control transport of ions and water for pollen germination during cross- and self-pollination.

Actin bundles, which were prominent in the papilla cells after cross-pollination, have also been observed in other plant cells, such as the pollen tube, the root hairs of *Hidrocharis*, and the stamen hair cells of *Tradescantia*. These actin bundles were involved not only in cytoplasmic streaming, but also in stabilizing the structure of transvacuolar strands and maintaining cellular morphology (Staiger et al., 1994; Shimmen et al., 1995; Tominaga et al., 2000). In the pollen tube of *Lilium longiflorum*, formation and structure of actin bundles are regulated by two villins, 135-ABP (for actin-binding proteins) and 115-ABP, in a Ca^{2+}/calmodulin-dependent manner (Yokota and Shimmen, 1999; Yokota et al., 2000, 2003; Hussey et al., 2006). Profilins, a family of G-ABPs, are associated with G-actin sequestration and Ca^{2+}-regulated actin polymerization and nucleation (Wasteneys and Yang, 2004). Thus, both the configuration of F-actin and actin dynamics are determined by the action of different ABPs and intracellular Ca^{2+} concentration regulates the activity of some of these proteins (Staiger, 2000; Hussey et al., 2006). In this study, actin polymerization and actin bundle formation were observed after cross-pollination, whereas actin reorganization and likely depolymerization were observed after self-pollination. Identification of ABPs, active in papilla cells during cross- and self-pollination, might, therefore, lead us to identify the mechanisms downstream of the SI signaling pathway.

In *Papaver rhoeas*, which has a gametophytic SI, the pollen *S*-phenotype is determined by its haploid *S*-genotype, and the female *S*-determinant is *S*-protein, which is expressed and secreted by cells of the stigma. When the pollen tube encounters the *S*-protein, pollen tube growth is inhibited in an *S*-haplotype-specific manner and actin cytoskeletal rearrangements in the pollen tube are integral to this process (Geitmann et al., 2000). Increases in intracellular [Ca^{2+}] precede actin rearrangements and an artificial increase in [Ca^{2+}] induces comparable actin cytoskeletal changes (Franklin-Tong et al., 2002; Snowman et al., 2002; Staiger and Franklin-Tong, 2003). These data suggest that [Ca^{2+}] is involved in the control of the actin cytoskeleton. Although the SI response in *B. rapa* is under sporophytic control, actin cytoskeleton rearrangements might also be triggered by increases in intracellular [Ca^{2+}]. During interactions between leguminous plants and *Rhizobium* and following treatment of root hair cells with Nod factor, a Ca^{2+} influx induces the rapid disappearance of actin from the tip region, suggesting that Ca^{2+} signaling can initiate the rapid depolymerization of actin (Cárdenas et al., 1998, 2003; Whitehead et al., 1998). Dynamic Ca^{2+} fluxes occur during pollen hydration, germination, and penetration following pollination in Arabidopsis (*Arabidopsis thaliana*; Iwano et al., 2004). It is possible that differences in actin reorganization detected in the papilla cells following cross- and self-pollination are caused by differences in quality or magnitude of Ca^{2+} signaling produced by cross- and self-pollen.

In this study, we showed that actin polymerization and actin bundle formation in the papilla cell are indispensable for pollen hydration and germination. We also showed that during the SI response, actin reorganization and likely depolymerization in the papilla cell prevent pollen germination and that the actin cytoskeleton is involved in controlling function and 3D structure of vacuoles in the papilla cells before and during self- and cross-pollination. Thus, understanding the regulation of actin dynamics in papilla cells is critical for a better understanding of the mechanisms at the heart of the SI response (i.e. the mechanisms that facilitate hydration of cross-pollen grains and inhibit hydration of self-pollen grains).

MATERIALS AND METHODS

Plant Growth Conditions

S^8-, S^9-, and S^{12}-allele homozygotes of *Brassica rapa* were cultivated in a greenhouse.

Sample Preparation for Rhodamine-Phalloidin Staining

The freshly opened flowers of an S^9 homozygote, of which the anthers were not dehisced, were excised and stuck to an agar plate. For cross-pollination, pollen grains from freshly dehisced anthers of S^{12} homozygotes were attached to the S^9 stigma. For self-pollination, pollen grains from S^9 homozygotes were attached. The pollinated stigma was analyzed 30, 60, or 90 min after pollination. For rhodamine-phalloidin staining, pistils were excised and treated with 250 μM freshly prepared *m*-maleimidobenzoyl *N*-hydroxysuccinimide ester (Sigma-Aldrich Chemie BV) in actin-stabilizing buffer (ASB; 100 mM PIPES, pH 6.8, 1 mM $MgCl_2$, 1 mM $CaCl_2$, and 75 mM KCl) for 1 min under vacuum and

incubated for 5 min under atmospheric conditions. These samples were subsequently fixed for 60 min with freshly prepared 4% formaldehyde in ASB. After samples were washed three times in ASB, the stigma was frozen in liquid nitrogen and crushed in an Eppendorf tube. The crushed sample was permeabilized with 0.05% Tween 20 in Tris-buffered saline containing dithiothreitol for 24 h and labeled with 500 nM rhodamine-phalloidin (Molecular Probes) in ASB. Specimens were washed with ASB before mounting with Vectar shield (Vectar Laboratories).

Transgene Constructs

The GFP2-mTalin expression cassette (Kost et al., 1998) was digested with *Xho*I, blunt ended with T4 DNA polymerase (TaKaRa), and digested with *Sac*I. This fragment was introduced into the *Sma*I-*Sac*I site of the SLG9 promoter-YC3.1 construct (Iwano et al., 2004) by replacing the YC3.1 coding sequence. This chimeric gene, comprising the 2.2-kb promoter region of the SLG9 gene, GFP2-mTalin coding sequence, and the nopaline synthase transcription terminator, was inserted into the binary vector pBI121 to create pSLG9mTn.

Transient Expression of GFP-mTalin

Transient expression of GFP-mTalin was performed as previously described (Murase et al., 2004).

Fluorescence Microscopy

Confocal laser-scanning microscopy was performed with a Zeiss LSM510 META (Zeiss). For rhodamine-phalloidin detection of actin, samples were scanned by He-Ne laser (543-nm excitation). Detection was performed using standard Texas Red filters (Zeiss) using a Zeiss 63× W Korr, 1.2 NA fluorescence objective and confocal optical sections were taken.

For GFP imaging, the samples were scanned by argon laser (488-nm excitation). A pistil was mounted on a coverslip prior to pollination, fixed with double-sided tape, and then covered with a piece of 1% agar. After a cross- or self-pollinating grain was mounted on a GFP-expressed papilla cell using a micromanipulator, GFP images were monitored under dry conditions using the microscope system described above.

Quantitative Assessment of Actin Rearrangements

For quantitative assessment of alterations in actin configuration, 3D images were obtained from the Z-series sections. Furthermore, fluorescence intensity for the cross section of the apical region in each papilla cell was measured and the mean value in each cell was calculated.

Statistical Analysis

The *t* tests were performed using the algorithm embedded into Microsoft Excel. The term significant is used in the text only when the change in question had $P < 0.05$.

High-Pressure Freezing and Freeze Substitution for Electron Microscopy

Stigmas before pollination and at 1 h after cross- and self-pollination were excised from styles and soaked in 10 μM CD for 4 h. These stigmas were transferred to gold sample holders, cryoprotected with hexadesin, frozen in a Baltec HPM 0101 high-pressure freezer, and transferred to liquid nitrogen. The samples were freeze substituted as reported previously (Iwano et al., 1999).

Ultra-HVEM, 3D Tomographic Reconstruction, and Modeling

For observation by ultra-HVEM, 2- to 3-μm-thick sections were cut and mounted on Formvar-coated copper slot grids. Sections were immersed in 3% uranyl acetate in 70% methanol, heated in a microwave oven for 30 s, incubated for 2 min at room temperature, and washed with water. The sections were then immersed in lead citrate, heated in a microwave oven for 30 s, incubated for 10 min at room temperature, and rinsed with water. Finally, the sections were coated on both sides with approximately 10 nm of evaporated carbon.

An ultra HVEM used was operated at 2,000 kV. Images were taken at 2,000× or 3,000× from +60° to −60° at 1° to 2° intervals around two orthogonal axes and collected with a 4K × 4K F415S CCD camera (TVIPS). The series were aligned and the tomographic volumes reconstructed as described (Mastronarde, 1997; McIntosh et al., 2005). The tomograms were displayed and modeled with the 3Dmod software package as described (Otegui et al., 2001; Segui-Simarro et al., 2004; McIntosh et al., 2005). For each tomography experiment, more than 100 different cells from more than 20 different stigmas were observed, and more than 100 electron micrographs were taken. Tomographic analysis of about 20 cells was performed.

Supplemental Data

The following materials are available in the online version of this article.

Supplemental Video S1. 3D structure of vacuoles in a papilla cell before pollination.

ACKNOWLEDGMENTS

We are grateful to Dr. Chua of Rockefeller University for his kind donation of pYSC14 and to Mr. Hasegawa, Mr. Takemura, Mrs. Onishi, Mrs. Yamamoto, Mrs. Matsumura, and Mrs. Ichikawa for their technical assistance.

Received December 26, 2006; accepted February 17, 2007; published March 2, 2007.

LITERATURE CITED

Bateman AJ (1955) Self-incompatibility systems in angiosperms. III. Cruciferae. Heredity **9:** 52–58

Cárdenas L, Thomas-Oates JE, Nava N, López-Lara IM, Hepler PK, Quinto C (2003) The role of Nod factor substituents in actin cytoskeleton rearrangements in *Phaseolus vulgaris*. Mol Plant Microbe Interact **16:** 326–334

Cárdenas L, Vidali L, Domínguez J, Pérez H, Sánchez F, Hepler PK, Quinto C (1998) Rearrangement of actin microfilaments in plant root hairs responding to *Rhizobium etli* nodulation signals. Plant Physiol **116:** 871–877

Dearnaley JDW, Clark KM, Heath IB, Lew RR, Goring DR (1999) Neither compatible nor self-incompatible pollinations of Brassica napus involve reorganization of the papillar cytoskeleton. New Phytol **141:** 199–207

Elleman CJ, Dickinson HG (1996) Identification of pollen components regulating pollination-specific responses in the stigmatic papillae of *Brassica oleracea*. New Phytol **133:** 1297–1305

Franklin-Tong VE, Holdaway-Clarke TL, Straatman KR, Kunkel JG, Hepler PK (2002) Involvement of extracellular calcium influx in the self-incompatibility response of *Papaver rhoeas*. Plant J **29:** 333–345

Geitmann A, Snowman BN, Emons AMC, Franklin-Tong VE (2000) Alterations in the actin cytoskeleton of pollen tubes are induced by the self-incompatibility reaction in *Papaver rhoeas*. Plant Cell **12:** 1239–1252

Hepler PK, Vidali L, Cheung AY (2001) Polarized cell growth in higher plants. Annu Rev Cell Dev Biol **17:** 159–187

Hussey PJ, Ketelaar T, Deeks MJ (2006) Control of the actin cytoskeleton in plant cell growth. Annu Rev Plant Biol **57:** 109–125

Iwano M, Shiba H, Funato M, Shimosato H, Takayama S, Isogai A (2003) Immunohistochemical studies on translocation of pollen *S*-haplotype determinant in self-incompatibility of *Brassica rapa*. Plant Cell Physiol **44:** 428–436

Iwano M, Shiba H, Miwa T, Che FS, Takayama S, Nagai T, Miyawaki A, Isogai A (2004) Ca^{2+} dynamics in a pollen grain and papilla cell during pollination of Arabidopsis. Plant Physiol **136:** 3562–3571

Iwano M, Wada M, Morita Y, Shiba H, Takayama S, Isogai A (1999) X-ray microanalysis of papillar cells and pollen grains in the pollination process in *Brassica* using a variable-pressure scanning electron microscope. J Electron Microsc **48:** 909–917

Kachroo A, Schopfer CR, Nasrallah ME, Nasrallah JB (2001) Allele-specific receptor-ligand interactions in Brassica self-incompatibility. Science **293:** 1824–1826

Kandasamy MK, Gilliland LU, McKinney EC, Meagher RB (2001) Plant actin isovariant, ACT7, is induced by auxin and required for normal callus formation. Plant Cell **13:** 1541–1554

Kobayashi I, Kobayashi Y, Hardham AR (1994) Dynamic reorganization of microtubules and microfilaments in flax cells during the resistance response to flax rust infection. Planta **195:** 237–247

Kobayashi I, Kobayashi Y, Yamaoka N, Kunoh H (1992) Recognition of a pathogen and a nonpathogen by barley coleoptile cells. III. Responses of microtubules and actin filaments in barley coleoptile cells to penetration attempts. Can J Bot **70:** 1815–1823

Kost B, Spielhofer P, Chua N-H (1998) A GFP-mouse talin fusion protein labels plant actin filaments in vivo and visualizes the actin cytoskeleton in growing pollen tubes. Plant J **16:** 393–401

Kutsuna N, Kumagai F, Sato MH, Hasezawa S (2003) Three-dimensional reconstruction of tubular structure of vacuolar membrane throughout mitosis in living tobacco cells. Plant Cell Physiol **44:** 1045–1054

Maeshima M (2001) Tonoplast transporters: organization and function. Annu Rev Plant Physiol Plant Mol Biol **52:** 469–497

Mastronarde D (1997) Dual-axis tomography: an approach with alignment methods that preserve resolution. J Struct Biol **120:** 343–352

McIntosh R, Nicastro D, Mastronarde D (2005) New views of cells in 3D: an introduction to electron tomography. Trends Cell Biol **15:** 43–51

Miller DD, De Ruijter NCA, Bisseling T, Emons AMC (1999) The role of actin in root hair morphogenesis: studies with lipochito-oligosaccharide as a growth stimulator and cytochalasin as an actin perturbing drug. Plant J **17:** 141–154

Mitsuhashi N, Shimada T, Mano S, Nishimura M, Hara-Nishimura I (2000) Characterization of organelles in the vacuolar-sorting pathway by visualization with GFP in tobacco BY-2 cells. Plant Cell Physiol **41:** 993–1001

Murase K, Shiba H, Iwano M, Che F-S, Watanabe M, Isogai A, Takayama S (2004) A membrane anchored protein kinase involved in *Brassica* self-incompatibility signaling. Science **303:** 1516–1519

Otegui MS, Mastronarde DN, Kang B-H, Bednarek SY, Staehelin LA (2001) Three-dimensional analysis of syncytial-type cell plates during endosperm cellularization visualized by high resolution electron tomography. Plant Cell **13:** 2033–2051

Reisen D, Francis Marty F, Nathalie Leborgne-Castel N (2005) New insights into the tonoplast architecture of plant vacuoles and vacuolar dynamics during osmotic stress. BMC Plant Biol **5:** 13

Saito C, Ueda T, Abe H, Wada Y, Kuroiwa T, Hisada A, Furuya M, Nakano A (2002) A complex and mobile structure forms a distinct subregion within the continuous vacuolar membrane in young cotyledons of *Arabidopsis*. Plant J **29:** 245–255

Schopfer CR, Nasrallah ME, Nasrallah JB (1999) The male determinant of self-incompatibility in *Brassica*. Science **286:** 1697–1700

Segui-Simarro JM, Austin II Jr, White EA, Staehelin LA (2004) Electron tomographic analysis of somatic cell plate formation in meristematic cells of Arabidopsis preserved by high-pressure freezing. Plant Cell **16:** 836–856

Shiba H, Takayama S, Iwano M, Shimosato H, Funato M, Takayama S, Isogai A (2001) A pollen coat protein, SP11/SCR, determines the pollen *S*-specificity in the self-incompatibility of *Brassica* species. Plant Physiol **125:** 2095–2103

Shimmen T, Hamatani M, Saito S, Yokota E, Mimura T, Fusetani N, Karaki H (1995) Roles of actin filaments in cytoplasmic streaming and organization of transvacuolar strands in root hair cells of *Hydrocharis*. Protoplasma **185:** 188–193

Shimmen T, Yokota E (2004) Cytoplasmic streaming in plants. Curr Opin Cell Biol **16:** 68–72

Silva NF, Stone SL, Christe LN, Sulaman W, Nazarain KAP, Burnett M, Arnoldo MA, Rothstein SJ, Goring DR (2001) Expression of the *S*-receptor kinase in self-compatible *Brassica napus* cv. Westar leads to the allele-specific rejection of self-incompatible *Brassica napus* pollen. Mol Gen Genet **265:** 552–559

Skalamera D, Heath MC (1998) Changes in the cytoskeleton accompanying infection-induced nuclear movements and the hypersensitive response in plant cells invaded by rust fungi. Plant J **16:** 191–200

Snowman BN, Kovar DR, Shevchenko G, Franklin-Tong VE, Staiger CJ (2002) Signal mediated depolymerization of actin in pollen during the self-incompatibility response. Plant Cell **14:** 2613–2626

Staiger CJ (2000) Signaling to the actin cytoskeleton in plants. Annu Rev Plant Physiol Plant Mol Biol **51:** 257–288

Staiger CJ, Franklin-Tong VE (2003) The actin cytoskeleton is a target of the self-incompatibility response in Papaver rhoeas. J Exp Bot **54:** 103–113

Staiger CJ, Yuan M, Valenta R, Shaw PJ, Warn RM, Lloyd CW (1994) Microinjected profilin affects cytoplasmic streaming in plant cells by rapidly depolymerizing actin microfilaments. Curr Biol **4:** 215–219

Stephenson AG, Doughty J, Dixon S, Elleman C, Hiscock S, Dickinson HG (1997) The male determinant of self-incompatibility in *Brassica oleracea* is located in the pollen coating. Plant J **12:** 1351–1359

Stone SL, Anderson EM, Mullen RT, Goring DR (2003) ARC1 is an E3 ubiquitin ligase and promotes the ubiquitination of proteins during the rejection of self-incompatible *Brassica* pollen. Plant Cell **15:** 885–898

Stone SL, Arnoldo M, Goring DR (1999) A breakdown of *Brassica* self-incompatibility in ARC1 antisense transgenic plants. Science **286:** 1729–1731

Sun H, Basu S, Brady SR, Luciano RL, Muday GK (2004) Interactions between auxin transport and the actin cytoskeleton in developmental polarity of *Fucus distichus* embryos in response to light and gravity. Plant Physiol **135:** 266–278

Takasaki T, Hatakeyama K, Suzuki G, Watanabe M, Isogai A, Hinata K (2000) The *S* receptor kinase determines self-incompatibility in *Brassica* stigma. Nature **403:** 913–916

Takayama S, Isogai A (2005) Self-incompatibility in plants. Annu Rev Plant Biol **56:** 467–489

Takayama S, Shiba H, Iwano M, Shimosato H, Che F-S, Kai N, Watanabe M, Suzuki G, Hinata K, Isogai A (2000) The pollen determinant of self-incompatibility in *Brassica campestris*. Proc Natl Acad Sci USA **97:** 1920–1925

Takayama S, Shimosato H, Shiba H, Funato M, Che F-S, Watanabe M, Iwano M, Isogai A (2001) Direct ligand-receptor complex interaction controls *Brassica* self-incompatibility. Nature **413:** 534–538

Takemoto D, Hardham AR (2004) The cytoskeleton as a regulator and target of biotic interactions in plants. Plant Physiol **136:** 3864–3876

Takemoto D, Jones DA, Hardham AR (2003) GFP-tagging of cell components reveals the dynamics of subcellular re-organization in response to infection of Arabidopsis by oomycete pathogens. Plant J **33:** 775–792

Tominaga M, Yokota E, Vidali L, Sonobe S, Hepler PK, Shimmen T (2000) The role of plant villin in the organization of the actin cytoskeleton, cytoplasmic streaming and the architecture of the transvacuolar strand in root hair cells of Hydrocharis. Planta **210:** 836–843

Wasteneys GO, Galway ME (2003) Remodelling the cytoskeleton for growth and form: an overview with some new views. Annu Rev Plant Biol **54:** 691–722

Wasteneys GO, Yang Z (2004) New views on the plant cytoskeleton. Plant Physiol **136:** 3884–3891

Whitehead LF, Day DA, Hardham AR (1998) Cytoskeletal arrays in the cells of soybean root nodules: the role of actin microfilaments in the organisation of symbiosomes. Protoplasma **203:** 194–205

Yokota E, Muto S, Shimmen T (2000) Calcium-calmodulin suppresses the filamentous actin-binding activity of 135-kilodalton actin-bundling protein isolated from lily pollen tubes. Plant Physiol **123:** 645–654

Yokota E, Shimmen T (1999) The 135-kDa actin-bundling protein from lily pollen tubes arranges F-actin into bundles with uniform polarity. Planta **209:** 264–266

Yokota E, Vidali L, Tominaga M, Tahara H, Orii H, Morizane Y, Hepler PK, Shimmen T (2003) Plant 115-kDa actin-filament bundling protein, P-115-ABP, is a homologue of plant villin and is widely distributed in cells. Plant Cell Physiol **44:** 1088–1099